

AXAF Science Center

Harvard-Smithsonian
Center for Astrophysics

MEMORANDUM

May 1, 1998

To: ASC, AXAF-CAT, AXAF Users
From: Deron Pease and Hank Donnelly
Subject: Count Rate Linearity of the
AXAF High Resolution Camera(HRC)

1 Introduction

The Count Rate Linearity (CRL) of the HRC characterizes the response of the detector micro-channel plates (MCPs) as a function of incident flux. When a photon is absorbed by a pore in an MCP, producing a cascade of electrons, the charge available for re-establishing the electric field in the pore is temporarily reduced. If the interval between photon absorptions in a given pore is shorter than the charge replenishment time, the electric field will not be completely re-established leading to a temporary, localized reduction in the gain. This in turn may lead to a reduction in the quantum efficiency, if the amount of charge detected from an event falls below the Lower Level Discriminator (LLD) cut off^[1].

For most normal operating conditions (flux < 2 cts/s/pore, or 5 cts/s in the focussed beam of AXAF), we expect the response of the detector to be linear requiring no correction. However, there remains the possibility via either serendipitous detections or transient phenomena that the normal operation limitation (5 cts/s^[2]) may be violated. This memo presents three analyses of the data collected at the XRCF for both the imaging and spectroscopic detectors (HRC-I and HRC-S), continuing the analysis presented in Kenter et al.^[3] and Kraft et al.^[4].

2 Count Rate Linearity Measurements

2.1 Setup and Procedure

At the X-Ray Calibration Facility (XRCF)^[5], CRL tests were performed by placing the HRC-I and HRC-S stationary at the focus of the HRMA (ie. no dithering). The CRL of both detectors was measured at energies of 0.277 keV using the Electron Impact Point Source(EIPS) with a carbon anode, and 2.56 keV using the Double Crystal Monochromator(DCM). Supplemental data for the HRC-S were also taken with the DCM at 3.5 keV. The incident source fluxes were monitored by four Flow Proportional Counters located around the perimeter of AXAF's High Resolution Mirror Assembly (HRMA) as Beam Normalization Detectors (BND-H's). Since the response of the BND-H's are linear throughout the count rate regime of these tests^[6], the measure of CRL is performed by directly comparing the HRC count rate versus the BND-H count rates. The range of rates obtained for the HRC-I and -S are outlined in Table 1.

Table 1: HRC Count Rates

Energy (keV)	HRC-I Rate Range (cts/s)	HRC-S Rate Range (cts/s)
0.277	3.1 – 19.8	0.5 – 19.0
2.560	2.1 – 6.4	0.5 – 5.4
3.500	—	3.7 – 19.3

2.2 The Data

The raw BND-H data were reduced to spectral line (ie. energy) count rates using the JMKMOD in XSPEC, as described in another ASC Memo [7]. The data were corrected for non-uniformities in the X-ray beam, using data supplied by John Everett (for the EIPS) and by Project Science (for the DCM). The effects of the beam uniformity corrections are quite noticeable. Figure 1 shows the data for the HRC-S at 0.277 keV before and after the correction was made. At this time, the BND-H's have not been calibrated absolutely. Thus, there still exist intrinsic variations among the four BND-H's. By first correcting for beam non-uniformities and then taking an ‘Average BND-H’, we are able to compensate for the small remaining variations and improve the overall signal-to-noise ratio of the BND-H count rates. We note that even with the application of the beam uniformity corrections and the calculation of an average BND-H, the errors in the BND-H data remain rather large, $\sim 5 - 10\%$.

The HRC count rates were calculated from the total counts within a 40 pixel radius and corrected for the live time of the test. We did *not* remove a background for the HRC, however we expect that the total contribution from this source to be negligible ($0.04 \text{ cts/s/cm}^2 \times 0.0021 \text{ cm}^2 = 8.31 \times 10^{-5} \text{ cts/s}$).

While the BND-H data (after fitting) represent only the data in the line, the HRC count rate includes response from any continuum photons present as well as those in the line of interest. Although the data taken using the DCM had no continuum component, we estimate that the continuum contribution for the EIPS source at 0.277 keV was $\sim 40\%$.

Although this is a significant component of the source count rate, we note two important characteristics about the EIPS continuum. First, for the case of the Carbon anode at 0.277 keV, the continuum extends only from the energy of the line up to $\sim 4 \times$ the line energy (i.e. 1.108 keV) which is the source voltage. Second because both line and continuum flux are determined by the current applied to the anode, the continuum flux should also increase proportionately to the line flux. Thus we are actually characterizing the CRL response in a band from slightly below 0.277 to 1.108 keV with an emphasis on the flux at 0.277 keV.

We also note that there is some uncertainty in the amount of background in the FPC's. Nominally, the total background over all of the channels should be $\sim 0.5 \text{ cts/s}$, and thus any error in the global background determination should be relatively small.

For the remainder of this report, we present the total count rate in HRC compared with the average, beam uniformity corrected, count rate in the line only from the BND-H's. A complete compilation of the data is found in Table 2. The data are available in an RDB table located at:

/data/aschrc5/pease/hrc.tex/CRL/data/hrc_crl_rates.rdb

3 Analysis

3.1 Comparison of Total Rates

The most direct method for investigating the CRL is a simple comparison of the total HRC count rates with the BND count rates (see Figures 2 and 3). We have attempted linear fits for all of the data sets and find excellent agreement with the data except for the highest count rate (~ 20 cts/s in the HRC-I) test performed at 0.277 keV. Excluding this data point significantly improved the quality of this particular fit. The fit results are shown as dotted lines on the plots, with solid lines connecting the data from point-to-point for comparison. The HRC-I shows a departure from non-linearity at the highest counting rate, while the HRC-S shows no evidence of non-linearity even at the highest rates (~ 20 cts/s). Nominally, this agrees with our expectations given that the Phillips plates used in the HRC-S have a lower resistance and thus will have a shorter charge replenishment time.

We note that while the relative placement of the data is correct, because of the effects mentioned above (HRC and FPC backgrounds, Continuum Contributions) the *absolute* placement is not. In other words, including one of the above effects would move the ensemble of points along one axis or the other, but would not affect the linear (or non-linear) nature of their relation. For this reason we have not forced the fits through the origin. In most cases (e.g. the DCM fits) the offset is small indicating that any potential effect is small.

3.2 Pulse-Height Amplitude Fitting

Photon absorption in the pores of the micro-channel plates results in temporary depletion of charge. The charge depletion manifests itself as temporary local depression in the gain of the detector. In turn, the lowered gain causes the Pulse Height Amplitude (PHA) distribution of events to shift to lower PHA channels.

In the absence of any other effects, a higher incident photon rate will cause a larger gain depression and thus a concomitantly larger shifting of the PHA distribution. However, the HRC is equipped with a Lower Level Discriminator (LLD) which rejects events below a set PHA channel. This is used to reduce/eliminate the noise that would otherwise be detected from the amplifiers. Count rate non-linearity occurs when, due to the temporarily depressed gain, real events fall below the LLD and are rejected.

For the PHA distribution from each CRL test, we fit a completely empirical function consisting of a ‘large x’ approximation Poisson function plus a Gaussian function of the form:

$$f_\mu(x) = A \left(e^{-(x-\mu)^2/2\mu} + Be^{-(x-\mu+C)^2/2\sigma^2} \right) \quad (1)$$

to the data. The ‘shape’ of the distribution – defined by σ , the Gaussian width, and C , the constant difference between the Poisson mean and the Gaussian mean – were fixed. This left a single parameter, μ , describing the “aggregate” location of the fit. Figure 4 show typical examples of our fits to the PHA.

We expect in the linear regime, as μ declines, that the shape of the PHA distribution will remain constant. When non-linearity occurs, i.e. the PHA distribution encounters the LLD, the quality of fit should degrade while the behavior of μ is uncertain, perhaps remaining relatively constant. Figure 5 shows the comparison of the fit, μ , versus the HRC rate for the 0.277 keV data with the HRC-I and HRC-S.

The value of μ for HRC-I declines as the rate increases, remaining constant at rates greater than 10 cts/s. At the same time χ^2 remains constant increasing at the same rate that μ stalls. For the HRC-S the data is less clear, and may indicate that the detector never enters the non-linear regime.

3.3 Core-Annulus Analysis

Due to the sharply peaked character of the AXAF Point-Spread-Function (PSF), the inner core region of the X-ray spot in an HRC image has a higher rate of photon incidence per pixel than the outer areas. Thus the charge depletion in the core region is greater than that in the wings. From this, we expect that the core may be a more sensitive indicator of non-linearity than the complete image.

The expected FWHM of the AXAF PSF is ~ 0.5 arcsec, or ~ 3.9 HRC pixels. The HRC has an intrinsic resolution element of $\sim 20\mu \simeq 3$ pixels. We defined the core region radius to be 3 pixels, thus including approximately 4 resolution elements. Smaller radii were rejected due to the poor statistics resulting from the low count rate. The annulus region was defined with an inner radius of 3 pixels and an outer radius of 8 pixels. This gives a reasonable representation for most of the counts in the PSF. Figure 6 shows an example of the focussed count rate linearity image with core and annulus regions indicated.

To facilitate comparison of the core and the annulus CRLs, the core data were normalized to the annulus data at the lowest count rate, as we expect the lowest rate to always fall within the linear regime of the detectors.

We find that, unlike the comparisons of the total count rates, at rates above 10 cts/s the core regions do appear to show noticeable divergences compared to the annuli (see Figures 7 through 8).

4 Results

We expect the counting behavior of the HRC (both I and S) to be linear for all normal operating conditions (< 5 cts/s). In fact even for serendipitous or accidental exposures to rates as high as 10 cts/s we expect that the detector response is linear.

Above these rates the significance of the departures from linearity is mixed. The total rate analysis for the HRC-I clearly demonstrates count rate non-linearity at the XRCF at rates above ~ 14 cts/s. The PHA fitting and Core-Annulus analyses suggest that the transition to non-linearity may begin at rates as low as 10 cts/s.

For the HRC-S, we find suggestive indications from the core-annulus studies that the HRC-S may also have demonstrated count rate non-linearities at rates above ~ 10 counts/s. This is *not* supported by the total rate analysis, while the PHA fitting analysis is inconclusive. As such the assertion of non-linearity for the HRC-S above 10 cts/s should be considered as tentative.

As a primitive empirical quantization of the HRC-I's behavior we have fit a quadratic function of the form:

$$Rate_{HRC-I} = 1.19 + 4.46 Rate_{BND} - 0.191 Rate_{BND}^2 \quad (2)$$

to the three highest rates observed with the EIPS data at 0.277 keV. Figure 9 shows the composite plot of the linear portion (dotted line) with the quadratic model fit (solid line). In a more useful form this becomes

$$True\ Rate_{HRC-I} = 45.91 - (2058.4 - 75.60 \times Obs.\ Rate_{HRC-I})^{1/2}. \quad (3)$$

A correction factor versus observed count rate in the HRC-I is shown in Figure 10. We expect that above ~ 24 cts/s the correction factor becomes *highly* unreliable and is indefinite above 27.2 cts/s, while below 12.2 cts/s we expect linear performance. We emphasize that any use of this correction factor should be done with extreme caution by the user.

References

- [1] SAO-HRC-DR-95-138, "High Resolution Camera: Science Instrument Operations Handbook"
- [2] ASC.TD.403, "AXAF Observatory Guide", October 1997
- [3] Kenter, A., Chappel, J.H., Kobayashi, K., Kraft, R.P., Meehan, G.R., Murray, S.S., Zombeck, M.V., Fraser, G.W., Pearson, J.F., Lees, J.E., Brunton, A.N., Pearce, S.E., Barbera, M., Collura, A. & Serio, S. "Performance and Calibration of the AXAF High Resolution Camera I: the Imaging Detector" *Proc. SPIE*,**3114**
- [4] Kraft, R.P., Chappel, J.H., Kenter, A., Kobayashi, K., Meehan, G.R., Murray, S.S., Zombeck, M.V., Fraser, G.W., Pearson, J.F., Lees, J.E., Brunton, A.N., Barbera, M., Collura, A. & Serio, S. "Performance and Calibration of the AXAF High Resolution Camera II: the Spectroscopic Detector" *Proc. SPIE*,**3114**
- [5] XCO Document, "XCO3: The HRMA/SI X-Ray Calibration Procedure"
- [6] Wargelin, B. 1998, ASC Memorandum, "Deadtime and Pileup Correction in the HXDS FPC's and SSD's"
- [7] Patnaude, D., Pease, D., and Donnelly, H. 1998, ASC Memorandum, "Phase G HRC Imaging BND Analysis"

Table 2: The HRC Count Rate Linearity Data

Test ID	Energy (keV)	HRC						BND-H		
		Total Rate cts s ⁻¹	Error cts s ⁻¹	Core Rate cts s ⁻¹	Error cts s ⁻¹	Annulus Rate cts s ⁻¹	Error cts s ⁻¹	Rate cts s ⁻¹	Error cts s ⁻¹	
G-IHI-CR-4.003	0.277	3.113	0.1152	1.093	0.0697	1.442	0.0795	0.389	0.0458	
G-IHI-CR-4.005	0.277	4.892	0.1620	1.547	0.0926	2.355	0.1133	0.931	0.0825	
G-IHI-CR-4.007	0.277	9.191	0.2106	3.027	0.1212	4.138	0.1413	1.973	0.1329	
G-IHI-CR-4.009	0.277	13.716	0.4566	4.321	0.2493	6.222	0.2997	3.214	0.2168	
G-IHI-CR-4.011	0.277	19.754	0.6692	5.738	0.3368	9.475	0.4392	5.433	0.3419	
G-IHS-CR-2.003a	2.560	2.153	0.0621	0.511	0.0311	1.185	0.0465	0.735	0.0559	
G-IHS-CR-2.005a	2.560	4.034	0.0903	1.005	0.0459	2.187	0.0669	1.587	0.1016	
G-IHS-CR-2.007a	2.560	6.424	0.1972	1.653	0.1017	3.256	0.1409	2.656	0.1875	
G-IHS-CR-4.002	0.277	0.496	0.0294	0.134	0.0161	0.259	0.0217	0.097	0.0150	
G-IHS-CR-4.004	0.277	1.998	0.0646	0.441	0.0314	1.168	0.0498	0.410	0.0406	
G-IHS-CR-4.006	0.277	4.300	0.1336	1.119	0.0697	2.292	0.0982	0.813	0.0727	
G-IHS-CR-4.008	0.277	7.962	0.2605	2.136	0.1359	4.121	0.1870	1.681	0.1328	
G-IHS-CR-4.010	0.277	12.250	0.3571	2.964	0.1738	6.679	0.2602	3.005	0.2019	
G-IHS-CR-4.012	0.277	19.020	0.7520	4.571	0.3394	9.898	0.5117	4.375	0.2549	
G-IHS-CR-1.004	2.560	0.455	0.0152	0.111	0.0078	0.236	0.0111	0.192	0.0175	
G-IHS-CR-2.004	2.560	1.905	0.0600	0.548	0.0330	0.981	0.0435	0.918	0.0648	
G-IHS-CR-2.006	2.560	5.397	0.1413	1.267	0.0698	3.032	0.1063	2.736	0.1618	
G-IHS-CR-99.062	3.500	3.698	0.1106	0.673	0.0488	1.948	0.0809	3.184	0.2108	
G-IHS-CR-99.063	3.500	7.318	0.2346	1.777	0.1171	4.811	0.1899	6.408	0.3969	
G-IHS-CR-99.064	3.500	19.292	0.4202	3.292	0.1689	11.462	0.3172	17.819	0.9733	

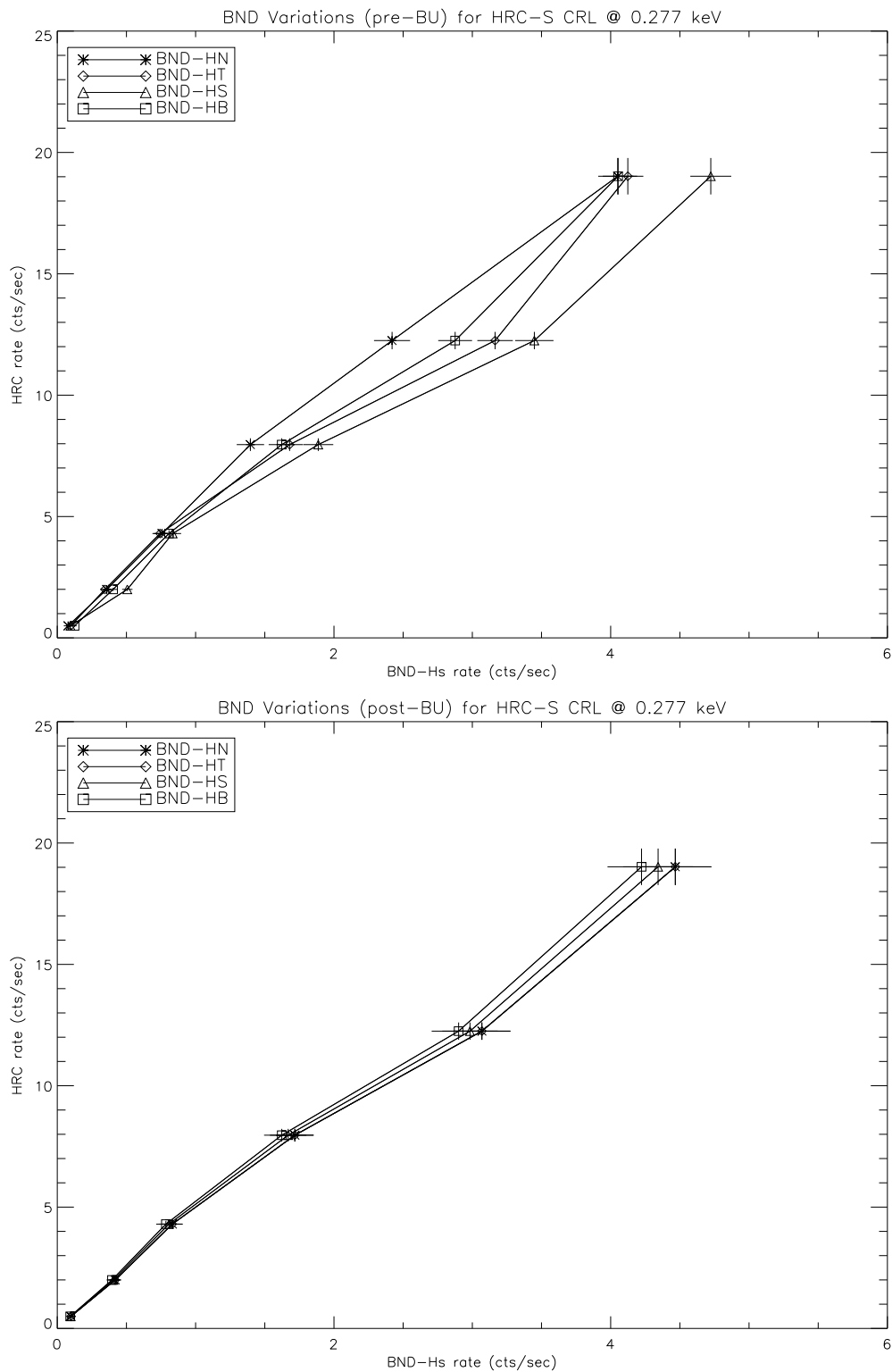


Figure 1: An example of the variations among the 4 BND-Hs. These plots show the HRC-S CRL at 0.277 keV as seen by all 4 BND-Hs before and after the application of the beam uniformity data. Note that the North and Top detectors show extremely good agreement.

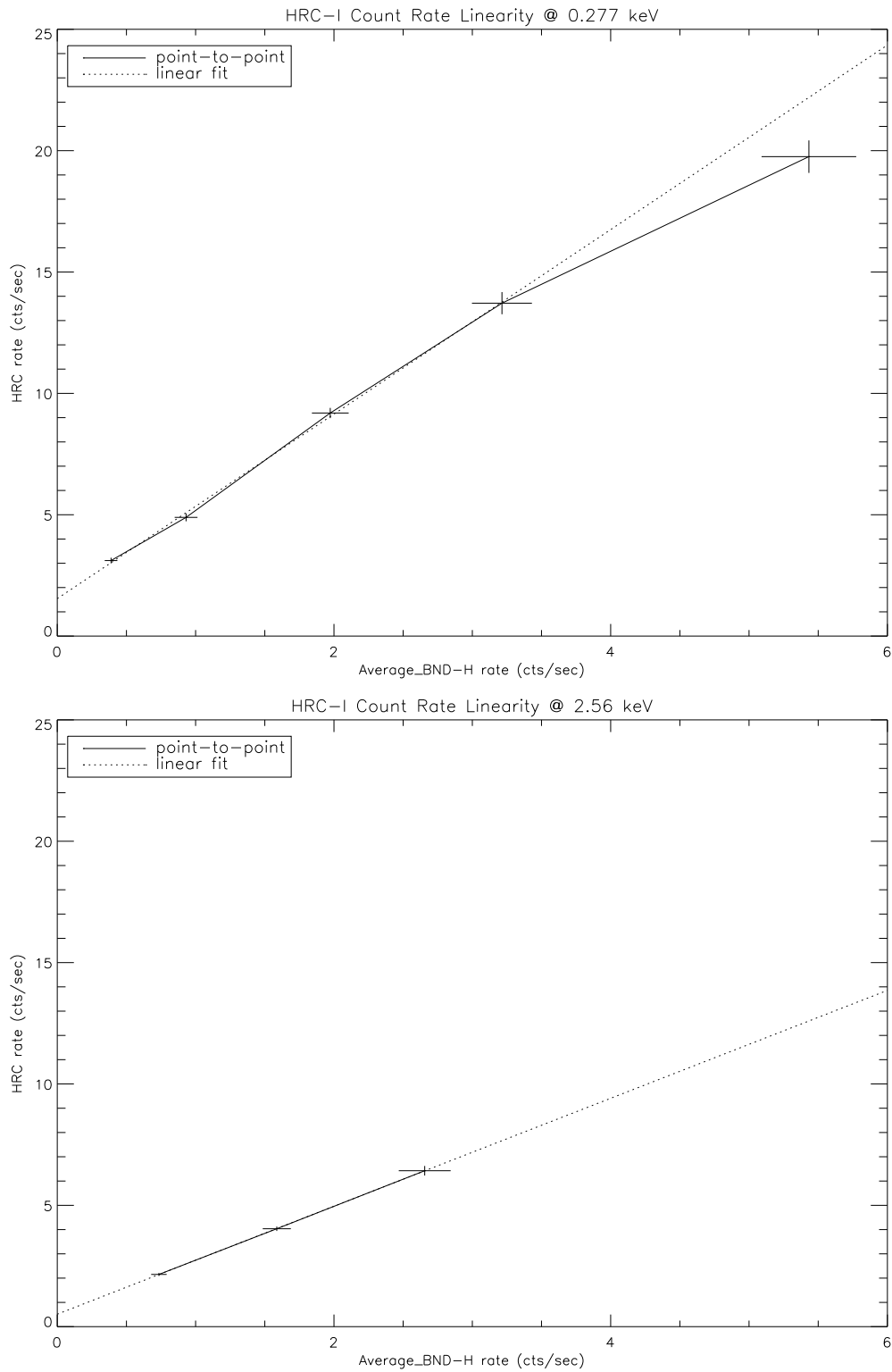


Figure 2: HRC-I count rate versus BND-H count rate (0.277 keV and 2.56 keV data sets). Solid lines are point-to-point; dotted lines represent linear model fits. Departure from linearity is apparent only in the 0.277 keV data set at the highest rate.

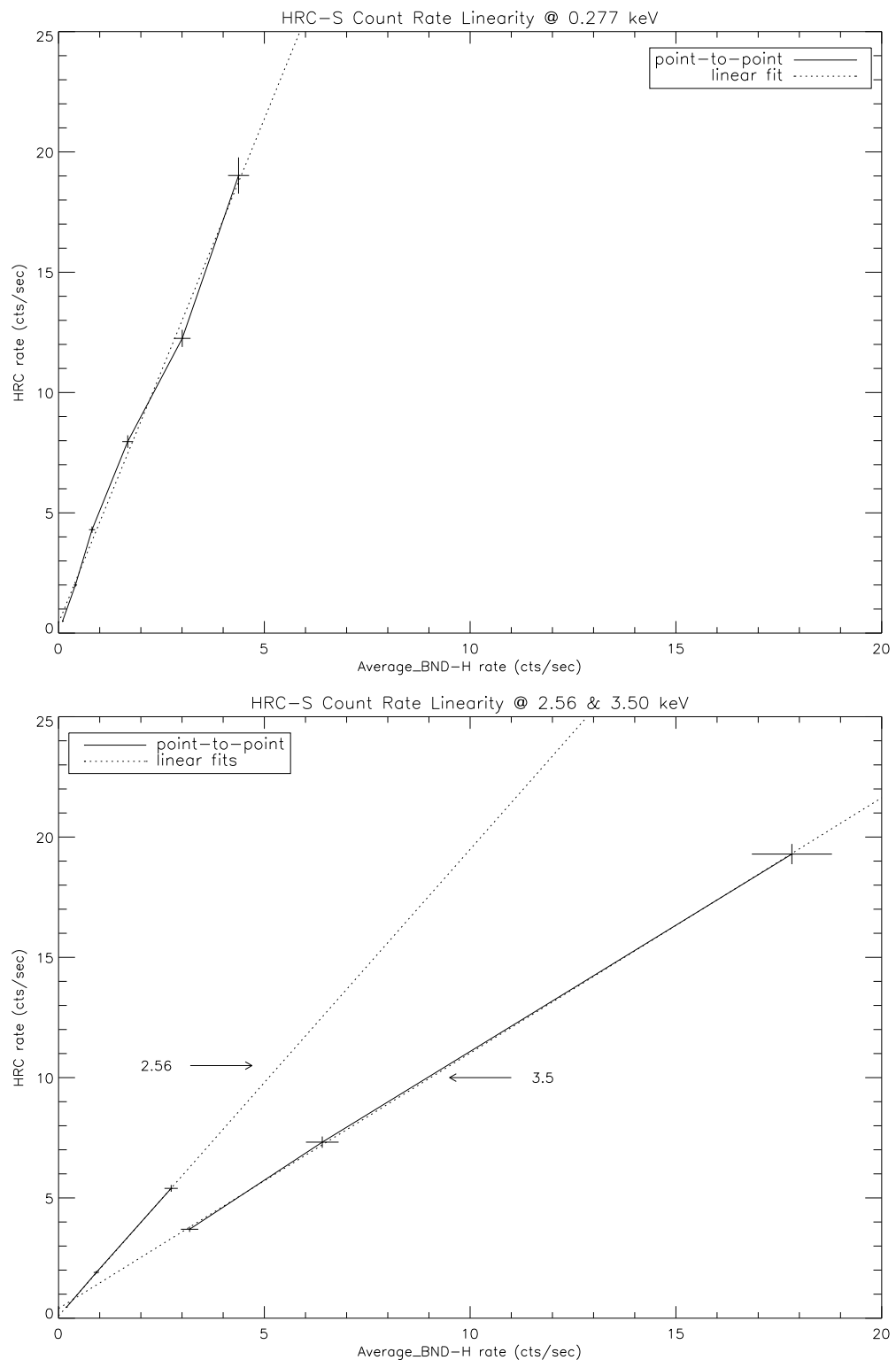


Figure 3: HRC-S count rate versus BND-H count rate 0.277 keV, 2.56 keV and 3.5 keV data sets. Solid lines are point-to-point; dotted lines represent linear model fits.

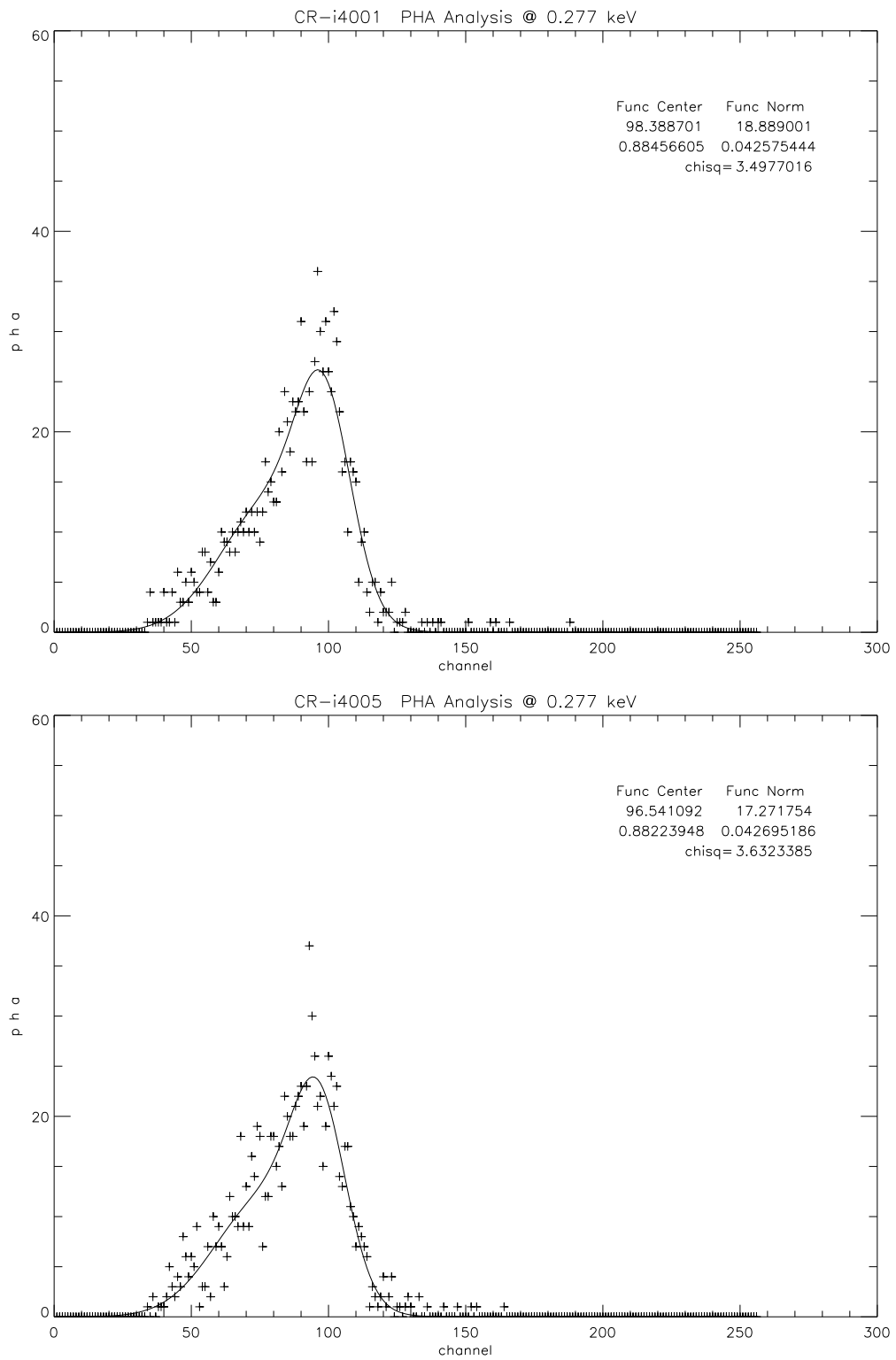


Figure 4: Examples of PHA distributions with Poisson+Gaussian function fits; HRC-I 0.277 keV data set. The Poisson mean μ is used to show the potential shift in the distribution to lower channels as a result of charge depletion on the MCPs.

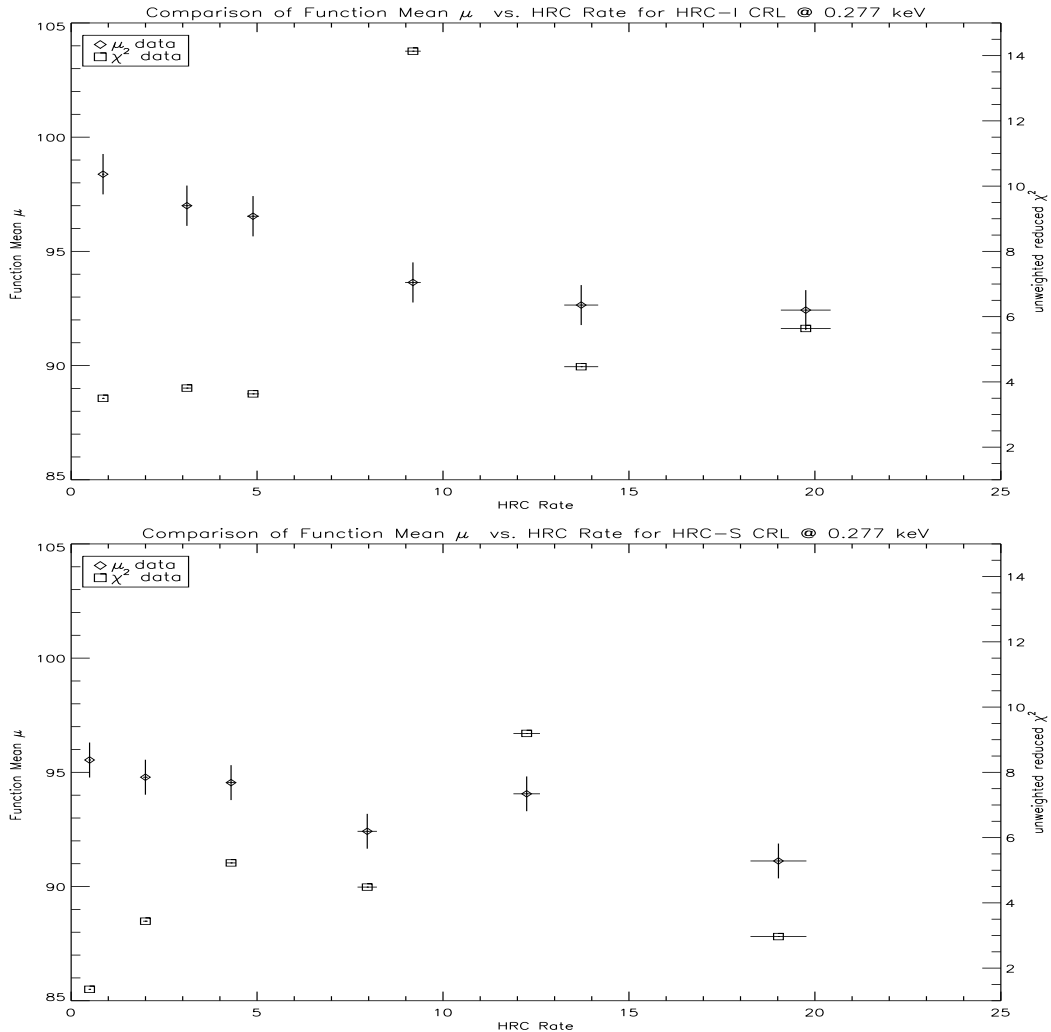


Figure 5: Comparison of the fit function value of μ to the count rate in the HRC-I and HRC-S at 0.277 keV. We expect to see μ decrease as incident rate increases. Also plotted are the χ^2 values for each fit.

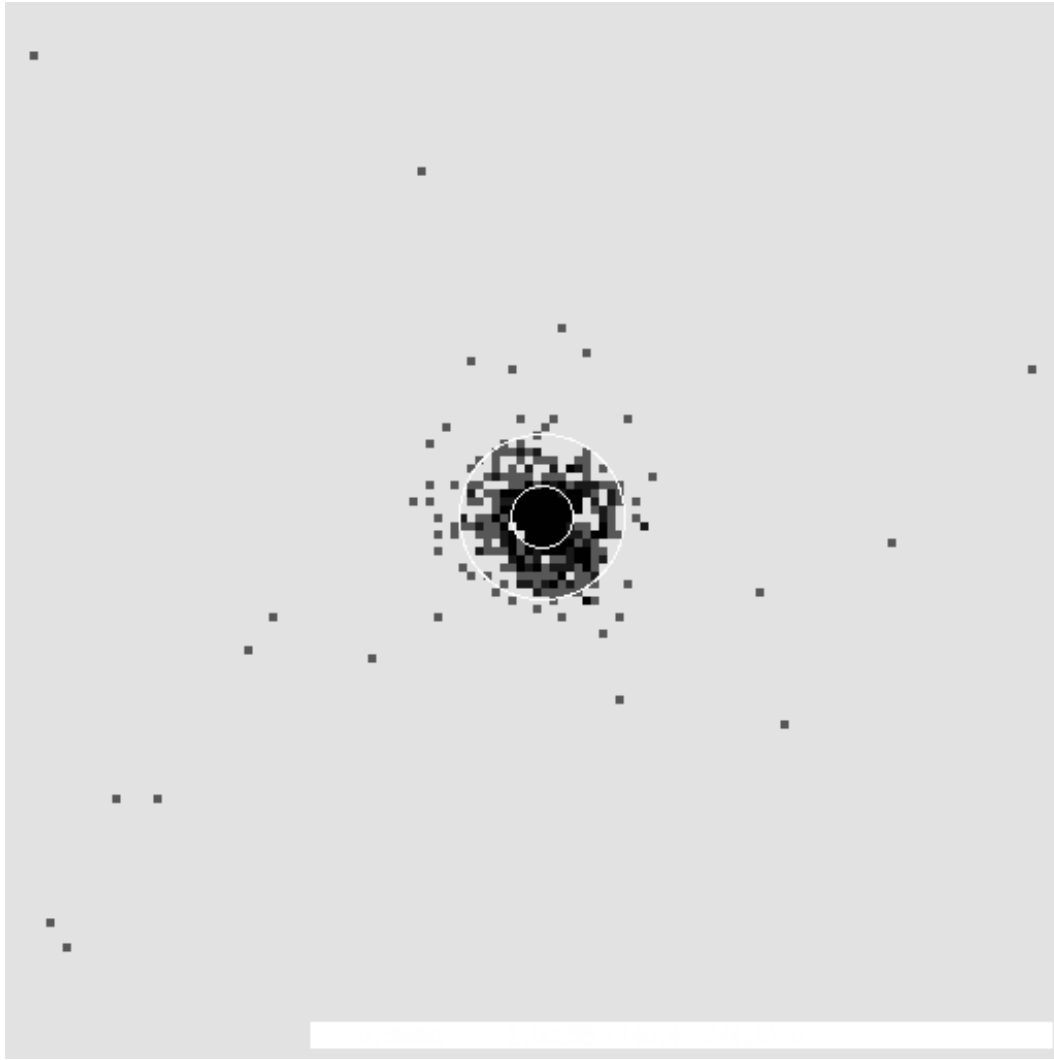


Figure 6: Example of the focussed count rate linearity image with core ($r = 3$ pixels) and annulus ($r_{inner} = 3$ pixels, $r_{outer} = 8$ pixels) regions shown; HRC-I 0.277 keV data set.

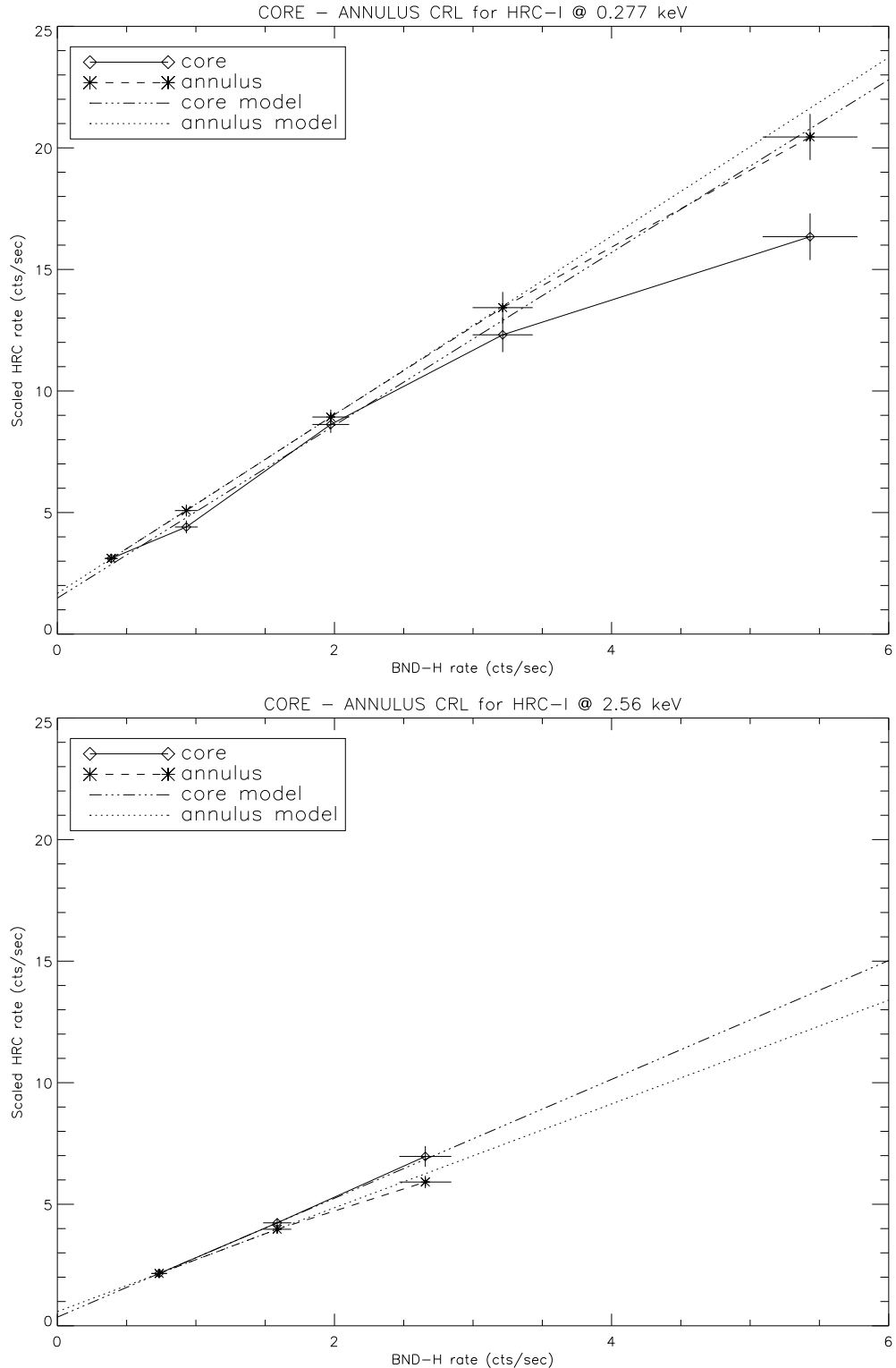


Figure 7: A comparison of the HRC-I count rate linearity in the core region with that in the annulus region at 0.277 keV and 2.56 keV. Solid lines are point-to-point for the core; dashed lines are point-to-point for the annulus; dash-dot-dot-dot lines are linear model fits to the core data; and dotted lines are linear model fits to the annulus data. Significant non-linearity in the core is apparent in the 0.277 keV data set.

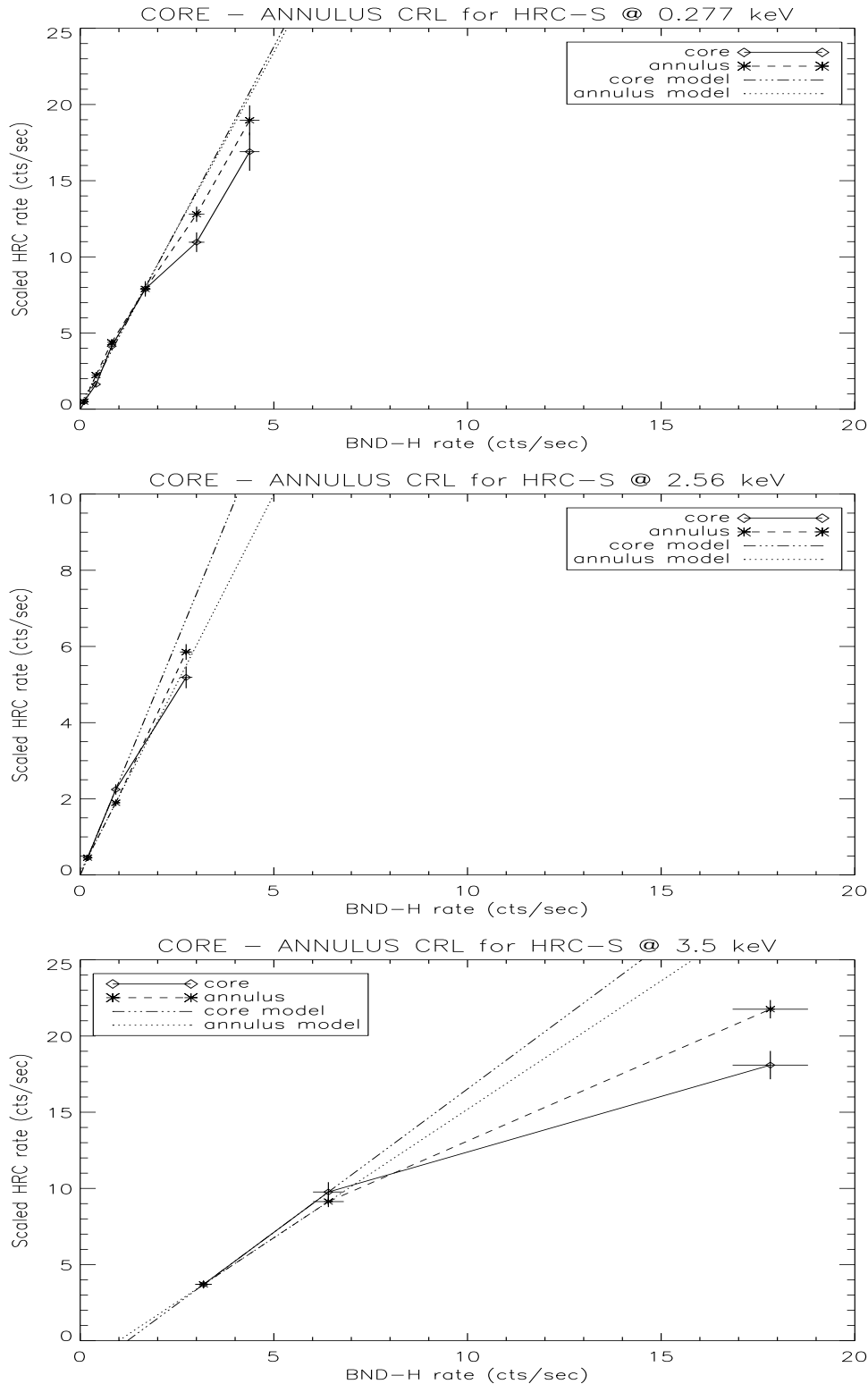


Figure 8: A comparison of the HRC-S count rate linearity in the core region with that in the annulus region at 0.277 keV, 2.56 keV and 3.5 keV. Solid lines are point-to-point for the core; dashed lines are point-to-point for the annulus; dash-dot-dot lines are linear model fits to the core data; and dotted lines are linear model fits to the annulus data. The data is suggestive of non-linearity in the core in the 0.277 keV and 3.5 keV data sets. Note augmented scale for data at 2.56 keV.

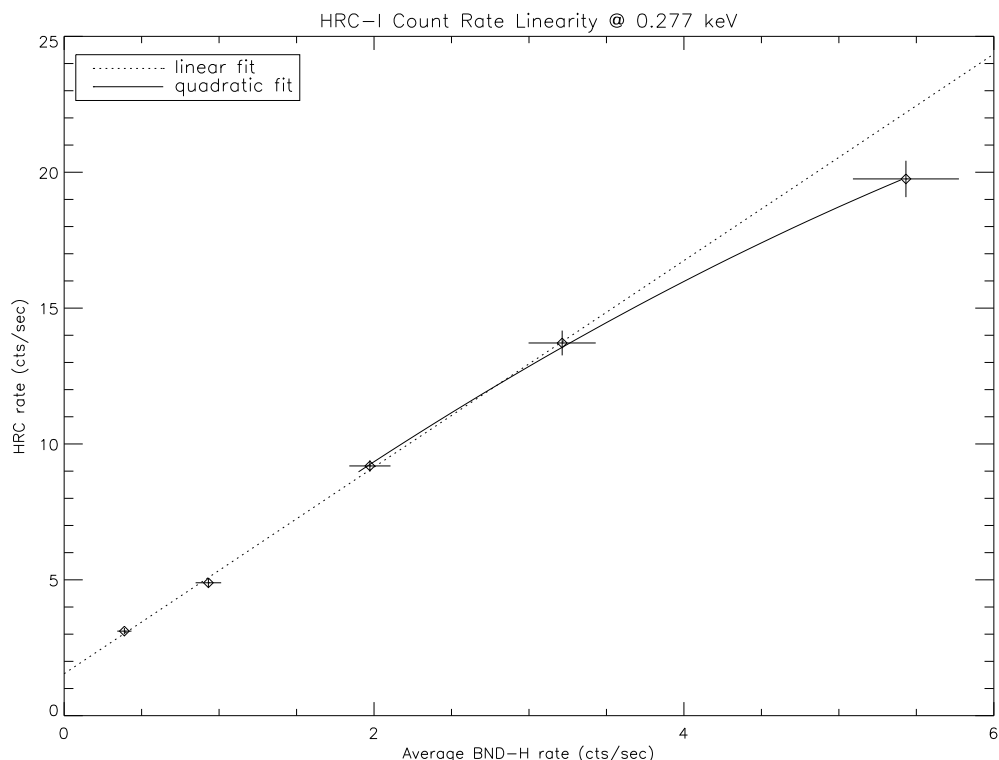


Figure 9: The linear (dotted line) + quadratic (solid line) fit to the HRC-I response to high rates achieved in the 0.277 keV data set. The equation of the quadratic part is $f(x) = 1.19 + 4.46x - 0.191x^2$.

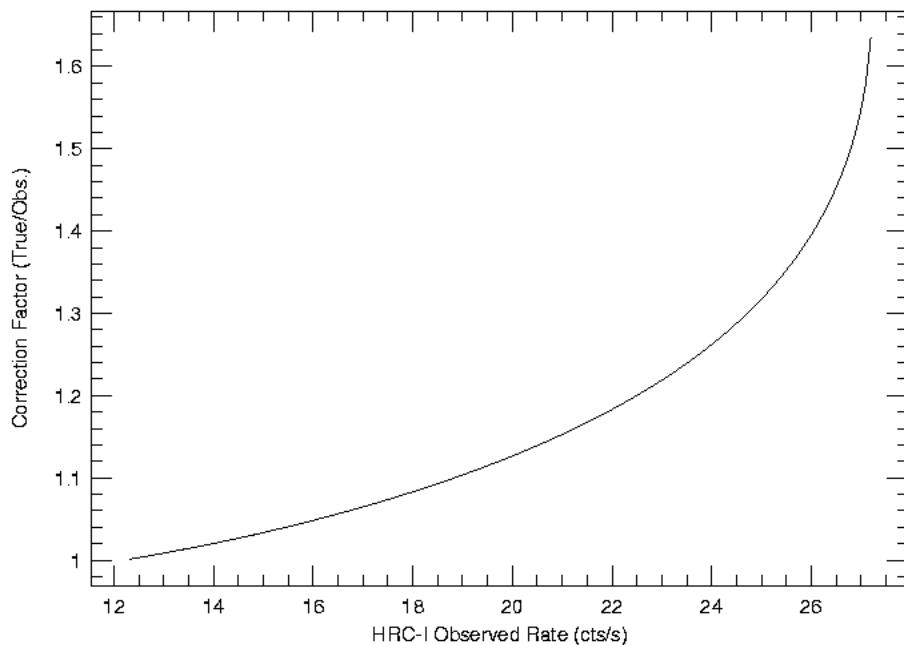


Figure 10: The correction factor to convert from observed count rate in the HRC-I to true incident count rate. Only rates below 27.3 cts/s are shown, as the correction factor becomes meaningless above these rates.